Selective Compensation of Distortion, Unbalanced and Reactive Power of a Thyristor-Controlled *LC*-Coupling Hybrid Active Power Filter (TCLC-HAPF)

Lei Wang, Chi-Seng Lam, *Senior Member, IEEE*, and Man-Chung Wong, *Senior Member, IEEE*

***Abstract*—When the load generated harmonic, unbalanced, and reactive power is beyond the limited capacity of a thyristor-controlled *LC*-coupling hybrid active power filter (TCLC-HAPF), the TCLC-HAPF with the conventional control methods cannot provide satisfactory compensation performance. In this paper, a selective compensation control method of harmonic distortion, unbalanced and reactive power of the TCLC-HAPF is proposed, which can function even at different voltage conditions (e.g., voltage dip, voltage fault, etc.). First, the proposed control method decomposes the load power into fundamental positive-sequence reactive power, fundamental negative-sequence power (unbalanced power), and harmonic power. Then, the decomposed reactive, unbalanced, and harmonic power can be selectively or fully compensated based on the capacity of the TCLC-HAPF. Finally, simulation and experimental results are provided to verify the effectiveness of the proposed selective compensation control method for the TCLC-HAPF.**

***Index Terms*—Negative-sequence active power, positive-sequence, reactive power, selective compensation, thyristor-controlled *LC*-coupling hybrid active power filter (TCLC-HAPF), unbalance power, voltage dip, voltage fault.**

I. Introduction

THE smart grid, regarded as the next-generation power grid, is considered as a promising solution for energy crisis. However, the smart grid is interconnected with different power grids, so that the different power quality problems can easily occur in weak grid areas such as harmonic distortion, lower power factor (PF), unbalanced problem, voltage dip, voltage fault, etc. The continuous development of the different power quality compensators has favored the developing progress of the smart grid. At the early stage, the passive power filters (PPFs) and static var compensators (SVCs) are used to solve the power quality problems. The PPFs are designed for the harmonic current and fixed reactive power compensation. And, the SVCs are designed for the dynamic reactive current and unbalanced power compensation [1]. However, both PPFs and SVCs are very sensitive to the voltage variation, and suffer from the resonance problem. The active power filters (APFs) can be used for solving the different power quality problems. However, their initial and operational costs are high. To reduce the power capacity of the active inverter part, hybrid APFs (HAPFs) have been proposed which combine the PPFs or SVCs in series/parallel with the APFs (PPF + APFs [2]–[6], PPF//APFs [7], [8], SVC//APFs [9]–[12], and SVC + APFs [13]–[17]). Among the different hybrid structures, the thyristor-controlled *LC*-coupling HAPF (TCLC-HAPF) [13]–[17] has the distinctive characteristics of a much wider compensation range than the series-connected structures of PPF + APFs and a lower dc-link voltage than the parallel-connected structures of PPF//APFs and SVC//APFs.

The above-mentioned APFs and HAPFs are normally designed as the global filters to compensate all the nonefficient power that is reactive, unbalanced, and harmonic power. However, due to the loads continuous expansion and the simultaneous operation of different loads, the global filters cannot provide satisfactory compensation performance if the targeted nonefficient power is beyond the designed capacity of the power filters. Therefore, it is suggested to selectively compensate the nonefficient power components (reactive, unbalanced, and harmonic power) when they are more than the compensation range of the power filters [18]–[26]. In [18]–[20], different harmonic selective compensation techniques are proposed. However, the reactive and unbalanced power has not been taken into consideration among those works. In [21], a selective compensation technique is proposed in distributed generators by inserting negative- and zero-sequence virtual impedances. However, the harmonic component compensation is not taken into account [21]. Steps beyond, the selective compensation of the nonefficient power components for the APF has been proposed by using the current decomposition approach [22], [23], equivalent con-

Manuscript received October 10, 2016; revised December 11, 2016; accepted January 10, 2017. Date of publication January 23, 2017; date of current version August 2, 2017. This work was supported in part by the Macau Science and Technology Development Fund (FDCT 109/2013/A3) and in part by the Research Committee of the University of Macau (MYRG2015-00030-AMSV, MYRG2015-00009-FST, MRG012/WMC/2015/FST). Recommended for publication by Associate Editor S. Golestan. *(Corresponding author: C.-S. Lam.)*

L. Wang is with the Department of Electrical and Computer Engineering, Faculty of Science and Technology, University of Macau, Macao, China.

C.-S. Lam is with the State Key Laboratory of Analog and Mixed Signal VLSI, University of Macau, Macao, China (e-mail: C.S.Lam@ieee.org; cslam@umac.mo).

M.-C. Wong is with the Department of Electrical and Computer Engineering, Faculty of Science and Technology and the State Key Laboratory of Analog and Mixed Signal VLSI, University of Macau, Macao, China.

Color versions of one or more of the figures in this paper are available online at http://ieeexplore.ieee.org.

Digital Object Identifier 10.1109/TPEL.2017.2656945

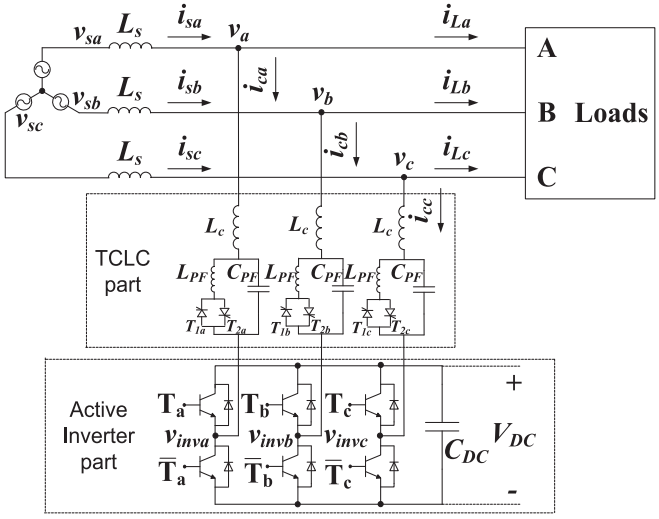

Fig. 1. Circuit configuration of the TCLC-HAPF.

ductance approach [24], IEEE Std. 1459-2000-based approach [25], and linear matrix inequalities approach [26]. However, all the above selective compensation methods [18]–[26] are developed for the APFs only. The selective compensation techniques for HAPFs especially for the SVC + APFs and the SVC//APFs still lack study. Moreover, the compensation performances under different voltage conditions such as voltage fault and voltage dip are not being considered too [18]–[26]. Therefore, this paper aims to develop a selective compensation control method for the TCLC-HAPF to selectively or fully compensate the harmonic distortion, unbalanced and reactive power components based on its designed capacity. And the proposed method can function well even under voltage dip or voltage fault condition.

In the following, the circuit configuration of the three-phase three-wire TCLC-HAPF is provided in Section II. And, the basic power analysis of the proposed selective compensation is illustrated in Section III. Then, the proposed selective compensation control method for the TCLC-HAPF is presented in Section IV. To verify the proposed selective control method, simulation case studies and representative experimental results are presented in Section V. Finally, conclusion will be drawn in Section VI.

II. Circuit Configuration of TCLC-HAPF

Fig. 1 shows the circuit configuration of the TCLC-HAPF, where *x* stands for phases *a*, *b,* and *c* in the following analysis. $v_{\rm sx}$ and v_x are the source and coupling point voltages, $i_{\rm sx}$, $i_{\rm Lx}$, and $i_{\rm cx}$ are the source, load, and compensating currents, respectively. L_s is the transmission line impedance. The TCLC-HAPF consists of a TCLC part and an active inverter part.

The TCLC part is composed of a coupling inductor L_c, a parallel capacitor $C_{\rm PF}$, and a thyristor-controlled reactor with $L_{\rm PF}$. The TCLC part provides a wide and continuous fundamental reactive power and unbalanced power compensation range, which is controlled by triggering the firing angles α of the thyristors [14].

The active inverter part is a voltage source inverter which consists of a dc-link capacitor $C_{\rm DC}$ and power switches insulated gate bipolar transistors (IGBTs). The small capacity of the active inverter part is used to compensate the harmonic power, avoid mistuning of the firing angles, and prevent the resonance problem of the TCLC part.

III. Power Analysis of the Proposed Selective Compensation

According to IEEE Std. 1459 [27], the definition of three-phase total effective apparent load power S_L in terms of the fundamental component and harmonic component can be expressed as

$$\begin{aligned} S_L^2 &= S_{L1}^2 + S_{\rm Lh}^2 \\ &= (3\cdot V_{L1}\cdot I_{L1})^2 + \Big[(3\cdot V_{L1}\cdot I_{\rm Lh})^2 \\ &\quad + (3\cdot V_{\rm Lh}\cdot I_{L1})^2 + (3\cdot V_{\rm Lh}\cdot I_{\rm Lh})^2\Big] \end{aligned} \tag{1}$$

where S_{L1} and $S_{\rm Lh}$ are the fundamental and harmonic components of the load apparent power. V_{L1}, I_{L1}, $V_{\rm Lh}$, and $I_{\rm Lh}$ are the fundamental and harmonic components of the load voltage and load current, respectively.

The fundamental load apparent power S_{L1} in (1) can be decomposed into positive-sequence component and unbalanced (negative) component [26], [27] as

$$S_{L1}^2 = \left(S_{L1}^+\right)^2 + \left(S_{U1}\right)^2 \tag{2}$$

where S_{L1}^+ is the positive-sequence component and S_{U1} is the unbalanced component of the apparent power.

Furthermore, the positive-sequence component S_{L1}^+ in (2) can be decomposed into the active power and reactive power as

$$\left(S_{L1}^+\right)^2 = \left(P_{L1}^+\right)^2 + \left(Q_{L1}^+\right)^2 \tag{3}$$

where P_{L1}^+ and Q_{L1}^+ are the fundamental load active power and reactive power. Based on (1)–(3), the load apparent power can be expressed as

$$S_L^2 = \left(P_{L1}^+\right)^2 + \left(Q_{L1}^+\right)^2 + \left(S_{U1}\right)^2 + \left(S_{\rm Lh}\right)^2. \tag{4}$$

In (4), the nonefficient power terms Q_{L1}^+, S_{U1}, and $S_{\rm Lh}$ are supposed to be compensated by the TCLC-HAPF. If those terms (Q_{L1}^+, S_{U1}, and $S_{\rm Lh}$) are falling within the TCLC-HAPF compensation range, the TCLC-HAPF can perform full compensation and only P_{L1}^+ will be left in the system source side. However, if the designed capacity ($S_{\rm TCLC-HAPF}$) of the TCLC-HAPF cannot fully compensate all the nonefficient power components, the selective compensation is needed to be performed, the expression of the TCLC-HAPF capacity is given as

$$S_{\rm TCLC-HAPF}^2 = \left(k_Q\cdot Q_{L1}^+\right)^2 + \left(k_U\cdot S_{U1}\right)^2 + \left(k_H\cdot S_{\rm Lh}\right)^2 \tag{5}$$

where k_Q, k_U, and k_H are the compensation ratio of Q_{L1}^+, S_{U1}, and $S_{\rm Lh}$, respectively. After the TCLC-HAPF compensation, the apparent power at the system source side can be expressed as

$$\begin{aligned} S_S^2 = &\left(P_{L1}^+\right)^2 + \left[(1-k_Q)\cdot Q_{L1}^+\right]^2 \\ &+ \left[(1-k_U)\cdot S_{U1}\right]^2 + \left[(1-k_H)\cdot S_{\rm Lh}\right]^2. \end{aligned} \tag{6}$$

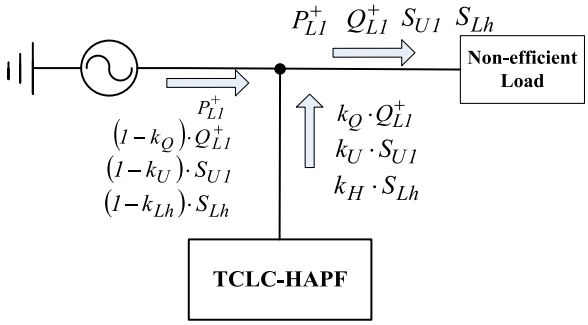

Fig. 2. Power flow of the proposed selective compensation of the TCLC-HAPF.

In (5) and (6), k_Q, k_U, and $k_H \in [0\ 1]$. However, if $S_{\mathrm{TCLC-HAPF}^2} \geq (Q_{L1}^{+})^2 + (S_{U1})^2 + (S_{\mathrm{Lh}})^2$, the TCLC-HAPF can perform full compensation with $k_Q = k_U = k_H = 1$ and $S_S = P_{L1}^{+}$. On the other hand, if $S_{\mathrm{TCLC-HAPF}}^2 < (Q_{L1}^{+})^2 + (S_{U1})^2 + (S_{\mathrm{Lh}})^2$, the selective compensation is needed with the tradeoff consideration among k_Q, k_U, and k_H.

Based on the above-mentioned discussions, the power flow of the proposed selective compensation of the TCLC-HAPF is illustrated in Fig. 2.

IV. Proposed Selective Compensation Control Strategy of the TCLC-HAPF

The TCLC-HAPF consists of the TCLC part and active inverter part. The TCLC part is controlled to provide a wide and continuous fundamental reactive power (Q_{L1}^{+}) and unbalanced power (S_{U1}) compensation range [14]. The low capacity active inverter part is mainly used to compensate the harmonic power (S_{Lh}) and also help to improve the performance of the TCLC part by enlarging its power compensation range. In the following, the control strategy of the TCLC-HAPF will be discussed in four parts:

A. active inverter part control,
B. TCLC part control,
C. compensation priority selection among k_Q, k_U, and k_H, and
D. the overall control block.

A. Active Inverter Part Control

The compensation principle of the active inverter part is to generate a reference compensating current $i_{\mathrm{cx}}{}^{*}$ to the controller, which includes the components of $k_Q Q_{L1}^{+}$, $k_U S_{U1}$, and $k_H S_{\mathrm{Lh}}$. By limiting the compensating current i_{cx} to track its reference value $i_{\mathrm{cx}}{}^{*}$, the TCLC-HAPF can cancel the harmonic current, balance the system, and compensate the reactive power to certain degree.

For the unbalanced three-phase three-wire system, the instantaneous v_x and i_{Lx} can be decomposed into the positive- and negative components by using the notch filter [28] as

$$\left[v_x^{+}(t)\right]_{x=a,b,c} = T_2 \cdot \left[v_x(t)\right]_{x=a,b,c} - T_1 \cdot \left[v_x^{D}(t)\right]_{x=a,b,c} \tag{7}$$

$$\left[i_{\mathrm{Lx}}^{+}(t)\right]_{x=a,b,c} = T_2 \cdot \left[i_{\mathrm{Lx}}(t)\right]_{x=a,b,c} - T_1 \cdot \left[i_{\mathrm{Lx}}^{D}(t)\right]_{x=a,b,c} \tag{8}$$

$$\left[i_{\mathrm{Lx}}^{-}(t)\right]_{x=a,b,c} = T_2 \cdot \left[i_{\mathrm{Lx}}(t)\right]_{x=a,b,c} + T_1 \cdot \left[i_{\mathrm{Lx}}^{D}(t)\right]_{x=a,b,c} \tag{9}$$

where $v_x(t)$ and $i_{\mathrm{Lx}}(t)$ are the three-phase load voltage and load current. $v_x^{D}(t)$ and $i_{\mathrm{Lx}}^{D}(t)$ can be obtained by delaying $v_x(t)$ and $i_{\mathrm{Lx}}(t)$ by 90°. $v_x^{+}(t)$ and $i_{\mathrm{Lx}}^{+}(t)$ are the positive sequence of the load voltage and current of each phase, $i_{\mathrm{Lx}}^{-}(t)$ is the negative sequence of the load current. T_1 and T_2 can be expressed as

$$T_1 = \frac{1}{2\sqrt{3}} \cdot \begin{bmatrix} 0 & 1 & -1 \\ -1 & 0 & -1 \\ 1 & -1 & 0 \end{bmatrix} \tag{10}$$

$$T_2 = \frac{1}{3} \cdot \begin{bmatrix} 1 & -0.5 & -0.5 \\ -0.5 & 1 & -0.5 \\ -0.5 & -0.5 & 1 \end{bmatrix}. \tag{11}$$

After obtaining $v_x^{+}(t)$, $i_{\mathrm{Lx}}^{+}(t)$, and $i_{\mathrm{Lx}}^{-}(t)$, the three-phase positive sequence and negative sequence active powers and reactive powers can be calculated as

$$\begin{bmatrix} p^{+} \\ \mathrm{q}^{+} \end{bmatrix} = \begin{bmatrix} v_\alpha^{+} & v_\beta^{+} \\ -v_\beta^{+} & v_\alpha^{+} \end{bmatrix} \cdot \begin{bmatrix} i_{\mathrm{L}\alpha}^{+} \\ i_{L\beta}^{+} \end{bmatrix} \tag{12}$$

$$\begin{bmatrix} p^{-} \\ q^{-} \end{bmatrix} = \begin{bmatrix} v_\beta^{+} & v_\alpha^{+} \\ -v_\alpha^{+} & v_\beta^{+} \end{bmatrix} \cdot \begin{bmatrix} i_{L\alpha}^{-} \\ i_{L\beta}^{-} \end{bmatrix}. \tag{13}$$

In (12) and (13), the positive and negative sequences of the voltage and current in the $\alpha - \beta$ plane are transformed from the *a-b-c* frames by

$$\begin{bmatrix} v_\alpha^{+} \\ v_\beta^{+} \end{bmatrix} = \begin{bmatrix} 1 & -1/2 & -1/2 \\ 0 & \sqrt{3}/2 & -\sqrt{3}/2 \end{bmatrix} \cdot \begin{bmatrix} v_a^{+} \\ v_b^{+} \\ v_c^{+} \end{bmatrix} \tag{14}$$

$$\begin{bmatrix} i_{L\alpha}^{+} \\ i_{L\beta}^{+} \end{bmatrix} = \begin{bmatrix} 1 & -1/2 & -1/2 \\ 0 & \sqrt{3}/2 & -\sqrt{3}/2 \end{bmatrix} \cdot \begin{bmatrix} i_{La}^{+} \\ i_{Lb}^{+} \\ i_{\mathrm{Lc}}^{+} \end{bmatrix} \tag{15}$$

$$\begin{bmatrix} i_{L\alpha}^{-} \\ i_{L\beta}^{-} \end{bmatrix} = \begin{bmatrix} 1 & -1/2 & -1/2 \\ 0 & \sqrt{3}/2 & -\sqrt{3}/2 \end{bmatrix} \cdot \begin{bmatrix} i_{La}^{-} \\ i_{Lb}^{-} \\ i_{\mathrm{Lc}}^{-} \end{bmatrix} \tag{16}$$

where $v_x^{+}(t)$ and $i_{\mathrm{Lx}}^{+}(t)$ are obtained from (7) to (9).

Referring to Fig. 2, $k_Q Q_{L1}^{+}$, $k_U S_{U1}$, and $k_H S_{\mathrm{Lh}}$ can be obtained as

$$\mathrm{k_Q} \cdot \mathrm{Q_{L1}^{+}} = \mathrm{k_Q} \cdot (\bar{q})^{+} \tag{17}$$

$$\mathrm{k_U} \cdot \mathrm{S}_{U1} = \mathrm{k_U} \cdot \sqrt{\left[(\bar{p})^{-}\right]^2 + \left[(\bar{q})^{-}\right]^2} \tag{18}$$

$$k_H \cdot S_{\mathrm{Lh}} = k_H \cdot \left(\sqrt{\left[(\tilde{p})^{+}\right]^2 + \left[(\tilde{q})^{+}\right]^2 + \left[(\tilde{p})^{-}\right]^2 + \left[(\tilde{q})^{-}\right]^2}\right)_{\mathrm{rms}}. \tag{19}$$

The detailed selection compensation among k_Q, k_U, and k_H will be explained in Section IV-C. By adding the scale factors (k_Q, k_U, and k_H) into the reference current calculation, the positive and negative compensating currents in $\alpha-\beta$ plane can be given as

$$\begin{bmatrix} i_{c\alpha}^{+} \\ i_{c\beta}^{+} \end{bmatrix} = \frac{1}{\left(v_{\alpha}^{+}\right)^2 + \left(v_{\beta}^{+}\right)^2} \cdot \begin{bmatrix} v_{\alpha}^{+} & -v_{\beta}^{+} \\ v_{\beta}^{+} & v_{\alpha}^{+} \end{bmatrix} \begin{bmatrix} k_H \cdot (\bar{p})^{+} \\ k_Q \cdot (\bar{q})^{+} + k_H \cdot (\tilde{q})^{+} \end{bmatrix} \quad (20)$$

$$\begin{bmatrix} i_{c\alpha}^{-} \\ i_{c\beta}^{-} \end{bmatrix} = \frac{1}{\left(v_{\alpha}^{+}\right)^2 + \left(v_{\beta}^{+}\right)^2} \cdot \begin{bmatrix} v_{\beta}^{+} & -v_{\alpha}^{+} \\ v_{\alpha}^{+} & v_{\beta}^{+} \end{bmatrix} \cdot \begin{bmatrix} k_U \cdot (\bar{p})^{-} + k_H \cdot (\tilde{p})^{-} \\ k_U \cdot (\bar{q})^{-} + k_H \cdot (\tilde{q})^{-} \end{bmatrix}. \quad (21)$$

The final reference compensating currents in the *a-b-c* plane are transformed from the $\alpha-\beta$ plane by

$$\begin{bmatrix} i_{\mathrm{ca}}^{*} \\ i_{\mathrm{cb}}^{*} \\ i_{\mathrm{cc}}^{*} \end{bmatrix} = \sqrt{\frac{2}{3}} \cdot \begin{bmatrix} 1 & 0 \\ -1/2 & \sqrt{3}/2 \\ -1/2 & -\sqrt{3}/2 \end{bmatrix} \cdot \begin{bmatrix} i_{c\alpha}^{+} + i_{c\alpha}^{-} \\ i_{c\beta}^{+} + i_{c\beta}^{-} \end{bmatrix}. \quad (22)$$

The active inverter part is used to improve the TCLC part compensation performance by limiting the compensating current i_{cx} to track with its reference value ${i_{\mathrm{cx}}}^{*}$. ${i_{\mathrm{cx}}}^{*}$ is calculated by the above proposed method and it is valid for different voltage and current conditions.

B. TCLC Part Control

The purpose of the TCLC part is to provide the reference compensating reactive power ${q_{\mathrm{cx}}}^{*}$ for each phase in order to compensate the reactive and unbalanced powers ($k_Q Q_{L1}^{+}$ and $k_U S_{U1}$) of the loading [14]. From the previous calculated reference compensating current ${i_{\mathrm{cx}}}^{*}$ which consists of the load reactive power, unbalanced and harmonic current components ($k_Q Q_{L1}^{+}$, $k_U S_{U1}$, and $k_H S_{\mathrm{Lh}}$), with the help of single-phase instantaneous *p-q* theory [29], v_x and ${i_{\mathrm{cx}}}^{*}$, the instantaneous reference compensating reactive power ${q_{\mathrm{cx}}}^{*}$ in each phase can be calculated as

$$\begin{bmatrix} q_{\mathrm{ca}}^{*} \\ q_{\mathrm{cb}}^{*} \\ q_{\mathrm{cc}}^{*} \end{bmatrix} = \begin{bmatrix} v_b \cdot i_{\mathrm{ca}}^{*D} - v_a^{D} \cdot i_{\mathrm{ca}}^{*} \\ v_b \cdot i_{\mathrm{cb}}^{*D} - v_b^{D} \cdot i_{\mathrm{cb}}^{*} \\ v_c \cdot i_{\mathrm{cc}}^{*D} - v_c^{D} \cdot i_{\mathrm{cc}}^{*} \end{bmatrix} \quad (23)$$

where v_x, ${i_{\mathrm{cx}}}^{*}$, ${v_x}^{D}$, and ${i_{\mathrm{cx}}}^{*D}$ are the load voltage, reference compensating current, and their values delay by 90°. Then, the reference compensating reactive power $Q_{\mathrm{cx}}^{*} \approx -\bar{q}_{\mathrm{cx}}^{*}/2$ can be obtained by using ${q_{\mathrm{cx}}}^{*}$ in (23) and three low pass filters (LPFs). With the calculated reference ${q_{\mathrm{cx}}}^{*}$, the required TCLC part impedance can be calculated as (24) shown at the bottom of this page, where $\bar{V}_x$ is the rms value of positive sequence phase voltage which can be instantaneous calculated by

$$\bar{V}_x = \|v\| \Big/ \sqrt{3} = \sqrt{v_a^{+2} + v_b^{+2} + v_c^{+2}} \Big/ \sqrt{3}. \quad (25)$$

Moreover, the expression of the TCLC impedances (X_{af}, X_{bf}, and X_{cf}) can also be expressed in terms of the TCLC part passive components and firing angles (α_x)

$$\begin{bmatrix} X_{\mathrm{af}}(\alpha_a) \\ X_{\mathrm{bf}}(\alpha_b) \\ X_{\mathrm{cf}}(\alpha_c) \end{bmatrix} = \begin{bmatrix} \dfrac{\pi X_{L_{\mathrm{PF}}} X_{C_{\mathrm{PF}}}}{X_{C_{\mathrm{PF}}}[2\pi - 2\alpha_a + \sin(2\alpha_a)] - \pi X_{L_{\mathrm{PF}}}} + X_{L_c} \\ \dfrac{\pi X_{L_{\mathrm{PF}}} X_{C_{\mathrm{PF}}}}{X_{C_{\mathrm{PF}}}[2\pi - 2\alpha_b + \sin(2\alpha_b)] - \pi X_{L_{\mathrm{PF}}}} + X_{L_c} \\ \dfrac{\pi X_{L_{\mathrm{PF}}} X_{C_{\mathrm{PF}}}}{X_{C_{\mathrm{PF}}}[2\pi - 2\alpha_c + \sin(2\alpha_c)] - \pi X_{L_{\mathrm{PF}}}} + X_{L_c} \end{bmatrix} \quad (26)$$

where X_{LPF}, X_{CPF}, X_{Lc} are the reactance of L_{PF}, C_{PF}, and L_c, respectively. The required X_{xf} in (24) is obtained by controlling the firing angle through (26). However, (26) does not have a closed-form solution. A look up table has been installed to directly obtain the firing angle α_x with known X_{xf}. By comparing the firing angle α_x with the phase angle $\varphi_{\mathrm{Vxf-Vnf}}$ of the voltage between TCLC part ($V_x - V_{\mathrm{nf}}$), the trigger signals to control the thyristors of the TCLC part can be obtained. The phase angle of the voltage between the TCLC part ($V_x - V_{\mathrm{nf}}$)

$$\begin{bmatrix} X_{\mathrm{af}} \\ X_{\mathrm{bf}} \\ X_{\mathrm{cf}} \end{bmatrix} = \begin{bmatrix} \dfrac{3 \cdot \bar{V}_x^2 \cdot (Q_{\mathrm{cc}}^{*} - Q_{\mathrm{cb}}^{*} - Q_{\mathrm{ca}}^{*})^{-1} \cdot (Q_{\mathrm{cb}}^{*} - Q_{\mathrm{ca}}^{*} - Q_{\mathrm{cc}}^{*})^{-1}}{(Q_{\mathrm{ca}}^{*} - Q_{\mathrm{cb}}^{*} - Q_{\mathrm{cc}}^{*})^{-1} + (Q_{\mathrm{cb}}^{*} - Q_{\mathrm{ca}}^{*} - Q_{\mathrm{cc}}^{*})^{-1} + (Q_{\mathrm{cc}}^{*} - Q_{\mathrm{cb}}^{*} - Q_{\mathrm{ca}}^{*})^{-1}} \\ \dfrac{3 \cdot \bar{V}_x^2 \cdot (Q_{\mathrm{ca}}^{*} - Q_{\mathrm{cb}}^{*} - Q_{\mathrm{cc}}^{*})^{-1} \cdot (Q_{\mathrm{cc}}^{*} - Q_{\mathrm{cb}}^{*} - Q_{\mathrm{ca}}^{*})^{-1}}{(Q_{\mathrm{ca}}^{*} - Q_{\mathrm{cb}}^{*} - Q_{\mathrm{cc}}^{*})^{-1} + (Q_{\mathrm{cb}}^{*} - Q_{\mathrm{ca}}^{*} - Q_{\mathrm{cc}}^{*})^{-1} + (Q_{\mathrm{cc}}^{*} - Q_{\mathrm{cb}}^{*} - Q_{\mathrm{ca}}^{*})^{-1}} \\ \dfrac{3 \cdot \bar{V}_x^2 \cdot (Q_{\mathrm{ca}}^{*} - Q_{\mathrm{cb}}^{*} - Q_{\mathrm{cc}}^{*})^{-1} \cdot (Q_{\mathrm{cb}}^{*} - Q_{\mathrm{ca}}^{*} - Q_{\mathrm{cc}}^{*})^{-1}}{(Q_{\mathrm{ca}}^{*} - Q_{\mathrm{cb}}^{*} - Q_{\mathrm{cc}}^{*})^{-1} + (Q_{\mathrm{cb}}^{*} - Q_{\mathrm{ca}}^{*} - Q_{\mathrm{cc}}^{*})^{-1} + (Q_{\mathrm{cc}}^{*} - Q_{\mathrm{cb}}^{*} - Q_{\mathrm{ca}}^{*})^{-1}} \end{bmatrix} \quad (24)$$

TABLE I
POWER QUALITY STANDARDS, EFFECTS AND PENALTY OF HARMONIC, UNBALANCED AND REACTIVE POWER PROBLEMS

		Harmonic power ($k_H\, S_{\mathrm{Lh}}$)	Unbalanced power ($k_U\, S_{U1}$)	Reactive power ($k_Q\, Q^+_{L1}$)
Related Standards	International	IEEE Std 519-2014 [30]	IEEE Std 1159-2009 [31]	N/A
	China	GB/T14595-93 [32]	GB/T 15543-2008 [33] GB755-87 [34]	Regulation of power factor adjusting charge [35]
	Requirements	$\mathrm{THD}_v < 5\%$ $\mathrm{THD}_i < 5-20\%$	$\mathrm{UF}_v < 0.5-2\%$ $\mathrm{UF}_i < 10\%$	$\mathrm{PF} > 0.8$
Effects		1) Damage to sensitive loads,	1) Reduce the transmission efficiency,	1) Increase rating of transformer and generator, and increase power loss,
		2) Resonance problem,	2) Increase power loss and temperature of transformer, etc.	2) Cause the voltage drop, etc.
		3) Increase power loss, etc.		
Penalty (GB standards)		Terminate electricity supply	Terminate electricity supply	Extra charge/cost

can be expressed as

$$\begin{bmatrix} \varphi_{\mathrm{Vaf-Vnf}} \\ \varphi_{\mathrm{Vbf-Vnf}} \\ \varphi_{\mathrm{Vcf-Vnf}} \end{bmatrix} = \begin{bmatrix} \theta_a - \tan^{-1}\left(\dfrac{X_{\mathrm{cf}} - X_{\mathrm{bf}}}{\sqrt{3}(X_{\mathrm{bf}} + X_{\mathrm{cf}})}\right) \\ \theta_b - \tan^{-1}\left(\dfrac{X_{\mathrm{af}} - X_{\mathrm{cf}}}{\sqrt{3}(X_{\mathrm{af}} + X_{\mathrm{cf}})}\right) \\ \theta_c - \tan^{-1}\left(\dfrac{X_{\mathrm{bf}} - X_{\mathrm{af}}}{\sqrt{3}(X_{\mathrm{bf}} + X_{\mathrm{af}})}\right) \end{bmatrix}_{\tan^{-1}\theta\in[-90^o,90^o]} \quad (27)$$

where θ_x is phase angle of the load voltage V_x, which can be obtained by using the phase lock loop. By comparing α_x with $\varphi_{\mathrm{Vxf-Vnf}}$, the trigger signals to control the thyristors of the TCLC part can be obtained.

C. Compensation Priority Selection Among k_Q, k_U, and k_H

In (17)–(19), $k_Q Q^+_{L1}$, $k_U S_{U1}$, and $k_H S_{\mathrm{Lh}}$ can be calculated. If the load reactive, unbalanced, and harmonic powers fall within the designed capacity of the TCLC-HAPF, the different power quality standards as shown in Table I can be satisfied simultaneously. However, if the designed capacity of the TCLC-HAPF is insufficient, the power quality standards may not be satisfied, and the compensation priority selection among reactive power, unbalanced, and harmonic currents can be done by changing the gains (k_Q, k_U, and k_H).

The compensation priority mainly depends on 1) power quality standards [30]–[35], 2) their effects, and 3) their corresponding penalty. Table I summarizes the power quality standards, effects and penalty of harmonic, and unbalanced and reactive power problems.

Based on Table I, if the harmonic current level is high, the harmonic sensitive loads can easily get damaged. And the resonance problem can also be caused by the harmonic current. Moreover,

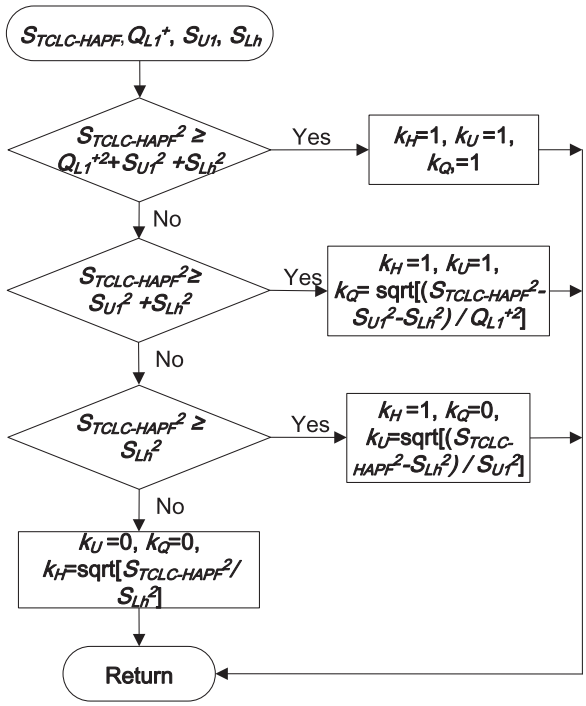

Fig. 3. Flowchart of the compensation priority assignments of k_Q, k_U, and k_H.

if the harmonic current level of the customer loads cannot satisfy the Chinese standard GB/T14595-93 [32], the electricity company has the right to terminate the electricity supply for that customer. In addition, the unbalanced voltage and current can reduce the transmission efficiency and increase the power loss and temperature of the transformer, etc. According to the Chinese standards GB/T 15543-2008 [33] and GB755-87 [34], the same penalty can be issued for unbalanced problem. On the other hand, the penalty of the reactive power problem in China is the extra charge, which is not as strict as the harmonic and unbalanced problems.

Based on the above-mentioned analysis, the compensation priority has been assigned to the gain of the harmonics k_H first,

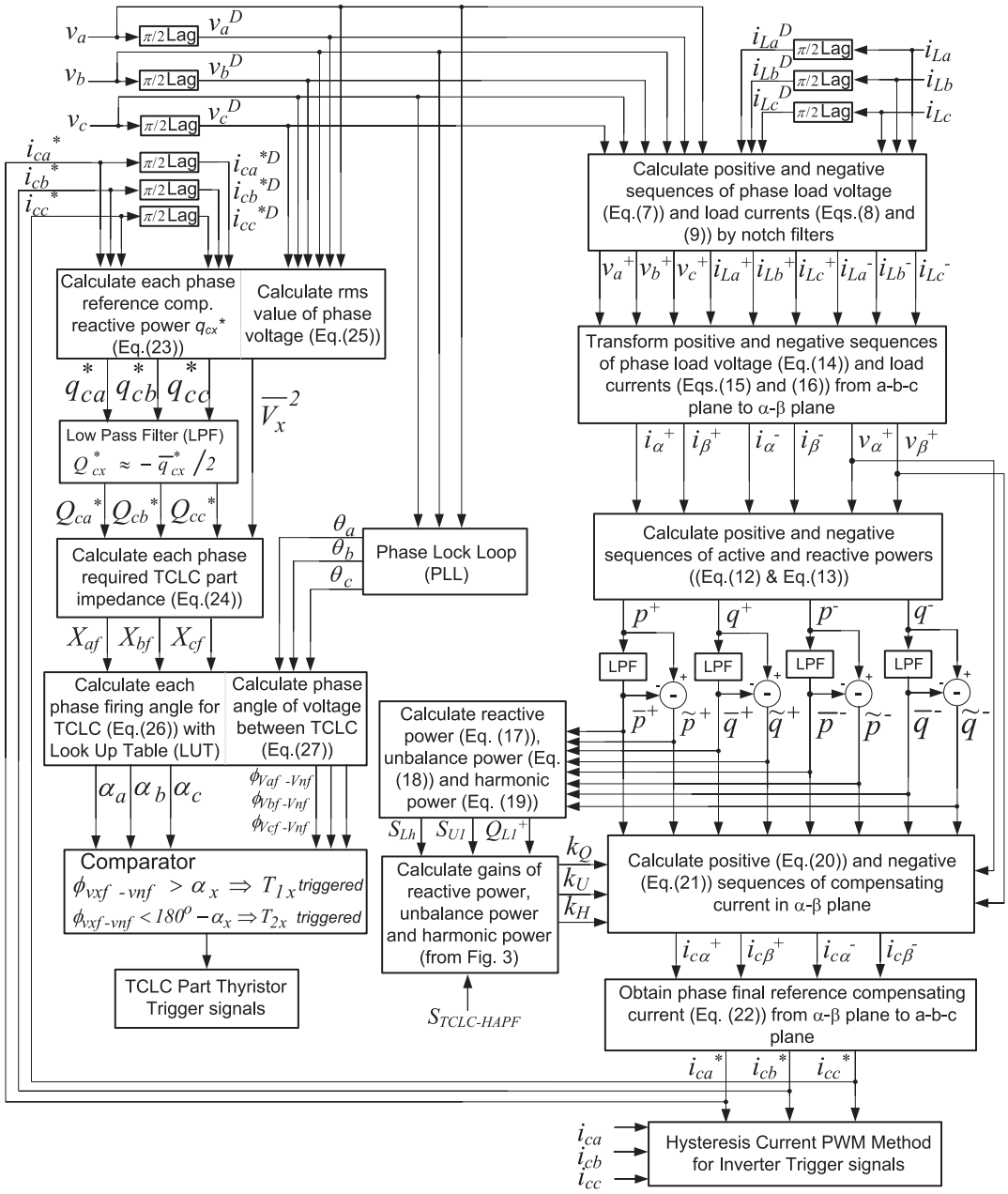

Fig. 4. Control block of the proposed selective compensation control strategy of TCLC-HAPF.

then to the gain of the negative sequence k_U, and the finally the gain of the reactive component k_Q in this paper. Certainly, users can also define their own compensation priority and compensation portion of each nonefficient power by themselves. The flowchart diagram to determine the gains (k_Q, k_U, and k_H) of the TCLC-HAPF is given in Fig. 3.

In Fig. 3, if k_H, k_U, and k_Q are equal to 1, the harmonic, unbalanced, and reactive powers are fully compensated. In contrast, if k_H, k_U, and k_Q are equal to 0 (no compensation), the harmonic, unbalanced, and reactive powers are not compensated. As shown in Fig. 3, if the TCLC-HAPF capacity $S_{\mathrm{TCLC-HAPF}}$ can compensate the load harmonic, unbalanced, and reactive powers simultaneously, $k_H = 1$, $k_U = 1$, and $k_Q = 1$. If $S_{\mathrm{TCLC-HAPF}}$ can fully support the harmonic and unbalanced powers compensation only, $k_H = 1$, $k_U = 1$, and $k_Q < 1$ (partial compensation). And if $S_{\mathrm{TCLC-HAPF}}$ can fully support the harmonic power compensation only, $k_H = 1$, $k_U < 1$, and $k_Q = 0$. Otherwise, if $S_{\mathrm{TCLC-HAPF}}$ cannot fully support the harmonic power compensation, $k_H < 1$, $k_U = 0$, and $k_Q = 0$. Based on Fig. 3, the gains k_Q, k_U, and k_H can be obtained correspondingly.

D. Control Block of the TCLC-HAPF

Fig. 4 shows the TCLC-HAPF overall control block diagram with the proposed selective compensation control strategy. Based on Fig. 4, it can be seen that the proposed selective

TABLE II
SIMULATION AND EXPERIMENTAL SYSTEM PARAMETERS FOR THE TCLC-HAPF POWER QUALITY COMPENSATION

	Parameters	Physical values
System parameters	V_x, f	110 V, 50 Hz
TCLC-HAPF parameters	L_c, $L_{\rm PF}$, $C_{\rm PF}$	5 mH, 30 mH, 160 μF
	$C_{\rm DC}$, $V_{\rm DC}$	5 mF, 80 V

compensation control strategy consists of the active inverter part control and the TCLC part control. The major connection between these two control loops is the calculated reference compensating current $i_{\rm cx}{}^*$. The reference current $i_{\rm cx}{}^*$ is calculated within the active inverter part control loop. And the target of the active inverter part instantaneously limits the compensating current $i_{\rm cx}$ to track with its reference value $i_{\rm cx}{}^*$, which includes the unwanted components of the loading fundamental reactive power $(k_Q Q_{L1}^+)$, unbalanced power $(k_U S_{U1})$, and harmonic power $(k_H S_{\rm Lh})$. The trigger signals for the active inverter part are generated by comparing $i_{\rm cx}$ and $i_{\rm cx}{}^*$ through the hysteresis current pulse width modulation method. On the other hand, the TCLC part control loop extracts the fundamental reactive power component from the reference current $i_{\rm cx}{}^*$. With the extracted reference compensating reactive power of each phase, the required TCLC part impedance can be calculated. Then, the corresponding trigger signals for the TCLC part in each phase can be generated based on the calculated TCLC part impedance.

V. SIMULATION AND EXPERIMENTAL VERIFICATIONS

To verify the proposed selective compensation control method among distortion, unbalanced, and reactive powers of the TCLC-HAPF, power systems computer aided design (PSCAD) simulation verifications are carried out to investigate the system performance under different voltage and current conditions. Moreover, a laboratory-scaled hardware prototype is also constructed to obtain the experimental results. The simulation and experimental system parameters for the TCLC-HAPF power quality compensation are shown in Table II.

The TCLC part is used to provide the $k_Q Q_{L1}^+$ and $k_U S_{U1}$ compensation. Therefore, the total amount of $k_Q Q_{L1}^+$ and $k_U S_{U1}$ provided by the TCLC part is given by

$$S_{\rm TCLCf} = 3 \cdot Q_{\rm cx\_TCLCf}(\alpha_x) = 3 \cdot \frac{\bar{V}_x^2}{X_{\rm TCLC}(\alpha_x)} = 3 \cdot \frac{\bar{V}_x^2}{\frac{\pi X_{L_{\rm PF}} X_{C_{\rm PF}}}{X_{C_{\rm PF}}[2\pi - 2\alpha_x + \sin(2\alpha_x)] - \pi X_{L_{\rm PF}}} + X_{L_c}} \quad (28)$$

where $\bar{V}_x$ is the rms value of the load voltage, X_{L_c}, $X_{L_{\rm PF}}$, and $X_{C_{\rm PF}}$ are the reactance of L_c, $L_{\rm PF}$, and $C_{\rm PF}$, respectively. When both thyristors are turned OFF for the whole fundamental period (firing angle $\alpha_x = 180°$), the TCLC part can provide the maximum capacitive compensating reactive power $Q_{\rm cx(MaxCap)}$. On the other hand, when one of the thyristors is alternately turned ON for half of the fundamental period (firing angle $\alpha_x = 90°$), the TCLC part can provide the maximum inductive compensating reactive power $Q_{\rm cx(MaxInd)}$ as $\alpha_x = 90°$. With the system parameters as shown in Table II and (28), the fundamental compensating reactive power range can be plotted in Fig. 5.

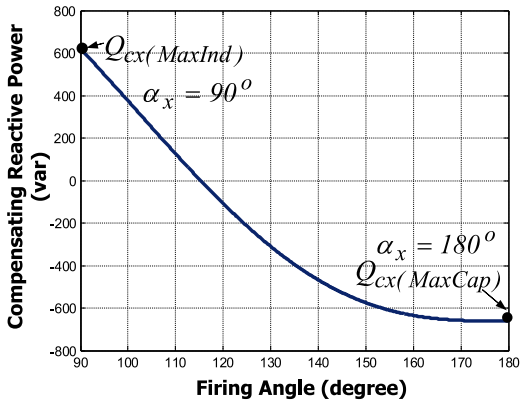

Fig. 5. Relationship between the firing angle and the compensating reactive power.

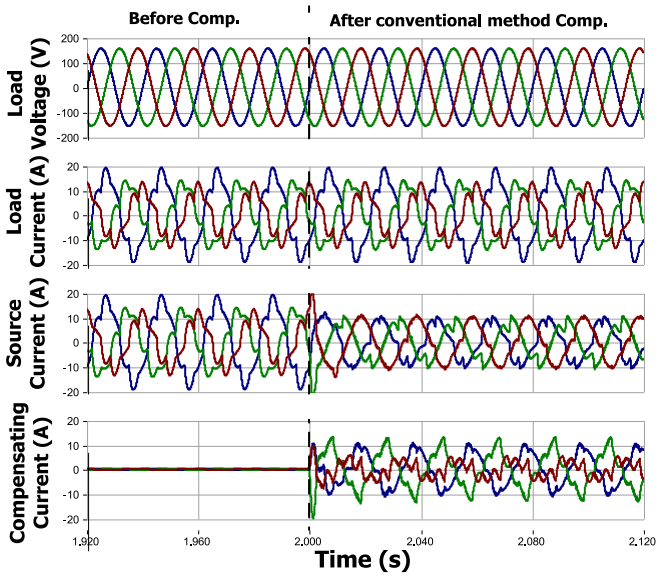

Fig. 6. Simulated distortion, unbalanced and reactive power compensation performances by using the conventional control strategy [14] of the TCLC-HAPF.

From Fig. 5, the maximum $k_Q Q_{L1}^+$ and $k_U S_{U1}$ powers provided by the TCLC part are $S_{\rm TCLCf\_max} = -3 \times 630\,{\rm var} = -1.89\,{\rm kvar}$ for inductive loading compensation and $S_{\rm TCLCf\_max} = 3 \times 600\,{\rm var} = 1.80\,{\rm kvar}$ for capacitive loading compensation.

Based on the capacity of the hardware components, the active inverter part is designed to be $S_{\rm Act} = 0.6$ kVA, which is mainly used for the harmonic current compensation and enlarging the $k_Q Q_{L1}^+$ and $k_U S_{U1}$ compensation range. In the following simulation and experimental case studies, the maximum capacity of the TCLC-HAPF is

$$S_{\rm TCLC-HAPF} = \sqrt{S_{\rm TCLCf\_max}^2 + S_{\rm Act}^2}. \quad (29)$$

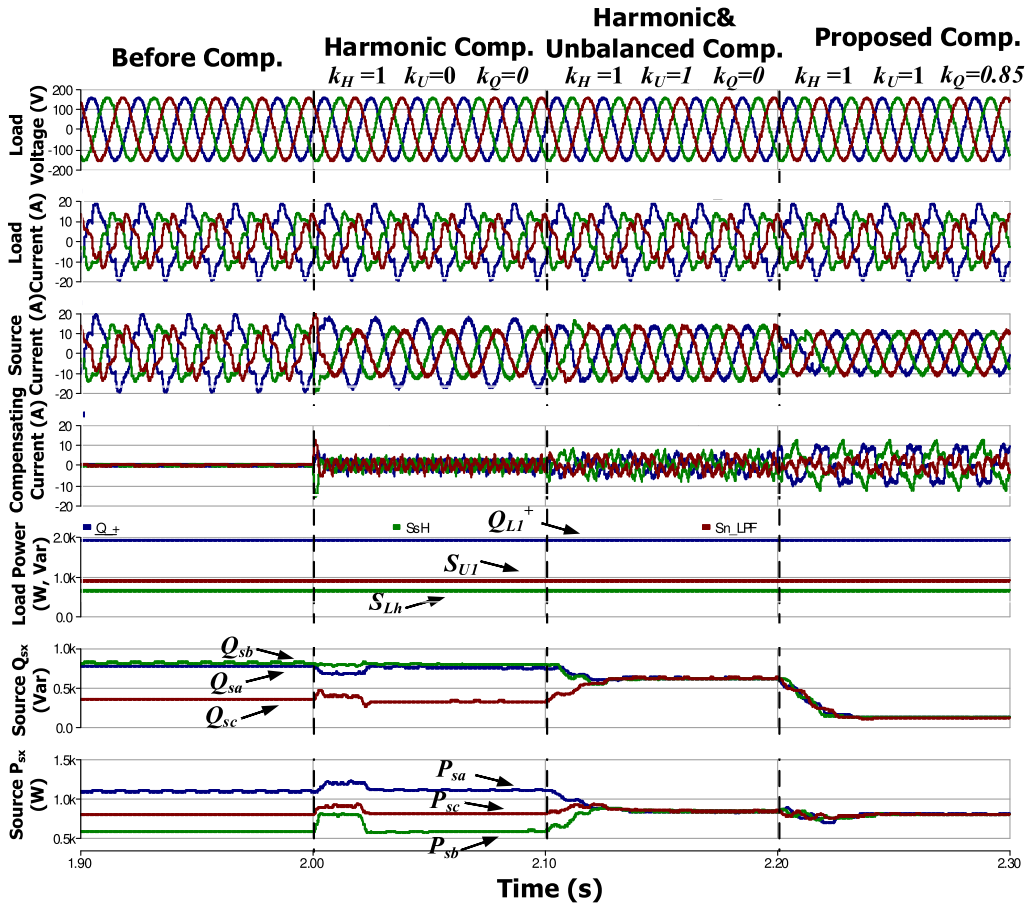

Fig. 7. Simulated distortion, unbalanced and reactive power compensation performances by using the proposed selective compensation control strategy of the TCLC-HAPF.

TABLE III
SIMULATION COMPENSATION RESULTS OF THE PROPOSED SELECTIVE COMPENSATION METHOD FOR THE TCLC-HAPF

	Phase	Q_{sx} (var)	PF	THD_{isx} (%)	UF_i (%)
Before Compensation	*a*	756	0.89	15.1	41.6
	b	809	0.57	21.5	
	c	346	0.81	24.5	
Conventional Method [14]	*a*	154	0.99	21.1	12.0
	b	64	0.96	27.2	
	c	44	0.96	13.3	
Proposed Method–Harmonic Compensation ($k_H = 1, k_U = 0, k_Q = 0$)	*a*	744	0.92	1.5	44.1
	b	800	0.59	2.8	
	c	330	0.83	2.6	
Proposed Method–Harmonic and Unbalanced Compensation ($k_H = 1, k_U = 1, k_Q = 0$)	*a*	612	0.81	2.3	1.2
	b	610	0.81	4.6	
	c	620	0.81	4.8	
Proposed Selective Compensation ($k_H = 1, k_U = 1, k_Q = 0.85$)	*a*	120	0.98	4.0	1.1
	b	124	0.98	3.9	
	c	118	0.98	5.9	
Proposed Selective Compensation during Voltage Dip	*a*	7	0.99	2.3	1.2
	b	9	0.99	2.7	
	c	8	0.99	2.5	

Based on (29) and the above-mentioned analysis, the maximum capacity of the TCLC-HAPF is designed to be $S_{\mathrm{TCLC-HAPF}} = 1.98$ kVA for inductive loading compensation and $S_{\mathrm{TCLC-HAPF}} = 1.90$ kVA for capacitive loading compensation. In this paper, with reference to the IEEE standard 519-2014 [30], the voltage THD_{vx} is required to be lower than 8% for the laboratory-scaled low-voltage application in this paper (<1 kV). For the IEEE standard 519-2014 [30], the acceptable total demand distortion (TDD) $\leq$ 12% with $I_{\mathrm{SC}}/I_{\mathrm{L}}$ in 50 $<$ 100 scale (a small capacity of isolated transformer used in the

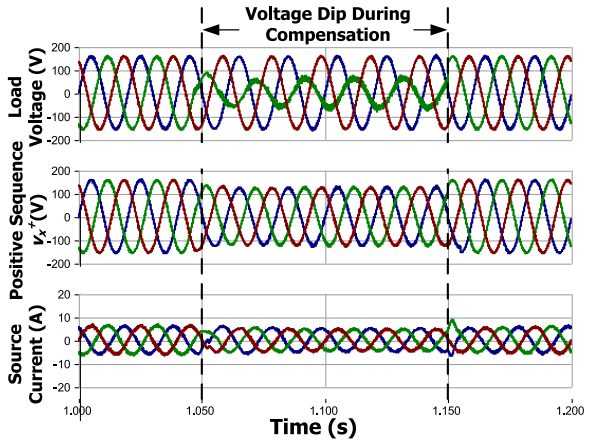

Fig. 8. Waveforms of v_x, its positive sequence v_x^+, and source current by using the proposed selective compensation control strategy of the TCLC-HAPF during voltage dip.

laboratory and a small rating 110 V-5 kVA experimental prototype). The nominal rated current is assumed to be equal to the fundamental load current at the worst-case analysis, which results in $\mathrm{THD} = \mathrm{TDD} \leq 12\%$. Therefore, this paper evaluates the TCLC-HAPF current harmonics compensating performance by setting an acceptable $\mathrm{THD_{isx}} \leq 12\%$.

A. PSCAD Simulations

The purpose of the simulation studies is to verify the conventional method [14] cannot provide satisfactory compensation results if the load generated noneffective powers are beyond the limited capacity of the TCLC-HAPF (in Fig. 6). With the same load, the proposed selective compensation control method for the TCLC-HAPF can selectively compensate distortion, unbalanced and reactive power components with the satisfactory results (in Fig. 7). Also, the proposed selective compensation method is verified under the voltage dip condition (in Fig. 8). The detailed compensation results are summarized in Table III.

In Fig. 6 and Table III, the TCLC-HAPF with the conventional method [14] can compensate the reactive power to 154, 64, and 44 var from the original 756, 809, and 346 var, and the source PF has been improved to 0.96 from the original 0.57 for the worst phase. However, the compensated $\mathrm{THD_{isx}}$ are 21.1%, 27.2%, and 13.3%, which cannot satisfy the IEEE standard 519-2014 [30]. This is due to the load noneffective powers are beyond the limited capacity of the TCLC-HAPF. On the other hand, from Fig. 7 and Table III, it can be seen that the proposed selective compensation method for the TCLC-HAPF can selectively compensate distortion, unbalanced and reactive power components. For harmonic compensation ($k_H = 1$, $k_U = 0$, $k_Q = 0$), the source active power and reactive power before and after the TCLC-HAPF compensation are basically keeping the same level. And the current unbalanced factor (UF_i) is still larger than >40% after compensation. However, the source current $\mathrm{THD_{isx}}$ has been compensated to 2.8% from the original 24.5% (worse phase among phases *a*, *b,* and *c*). For both harmonic and unbalanced compensation ($k_H = 1$, $k_U = 1$, $k_Q = 0$), UF_i is reduced to 1.2% from the original 41.6%. And the source reactive power (Q_{sx}) and active power (P_{sx}) of each phase become the same. Meanwhile, $\mathrm{THD_{isx}}$ has been compensated to be lower than 5%. For the proposed selective compensative method ($k_H = 1$, $k_U = 1$, $k_Q = 0.85$), the source PF and UF_i are improved to 0.98 and 1.1, respectively. And, $\mathrm{THD_{isx}}$ is compensated to 5.9% (worst phase). In addition, there is still remaining Q_{sx} value which is due to the gain $k_Q = 0.85$ instead of $k_Q = 1$.

From Fig. 8 and Table III, it can be seen that the positive sequence of the load voltage v_x^+ can be instantaneously extracted by using (7). The source PF and $\mathrm{THD_{isx}}$ can be compensated to 0.99 and 2.7% (worse phase) even during the voltage dip condition.

Fig. 9. Experimental setup of the TCLC-HAPF hardware prototype and its testing environment.

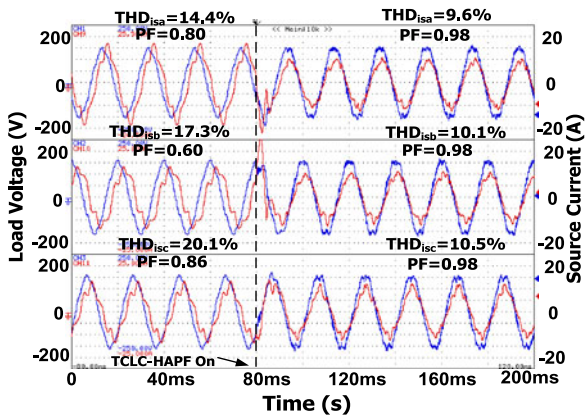

Fig. 10. Experimental waveforms of v_x and i_{sx} before and after the TCLC-HAPF compensation with the proposed selective compensation method ($k_H = 1$, $k_U = 1$, $k_Q = 0.85$).

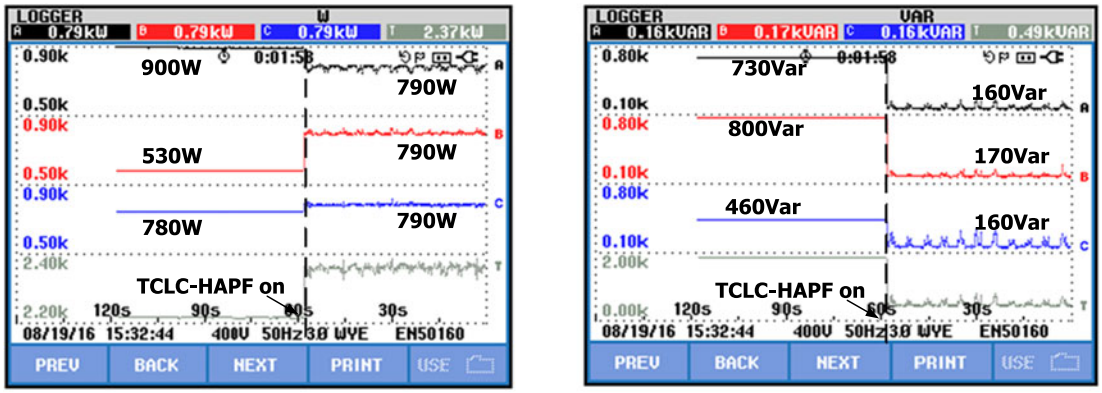

(a) (b)

Fig. 11. Experimental results of dynamic performance before and after the TCLC-HAPF compensation with the proposed selective compensation method ($k_H = 1$, $k_U = 1$, $k_Q = 0.85$): (a) $P_{\rm sx}$ and (b) $Q_{\rm sx}$.

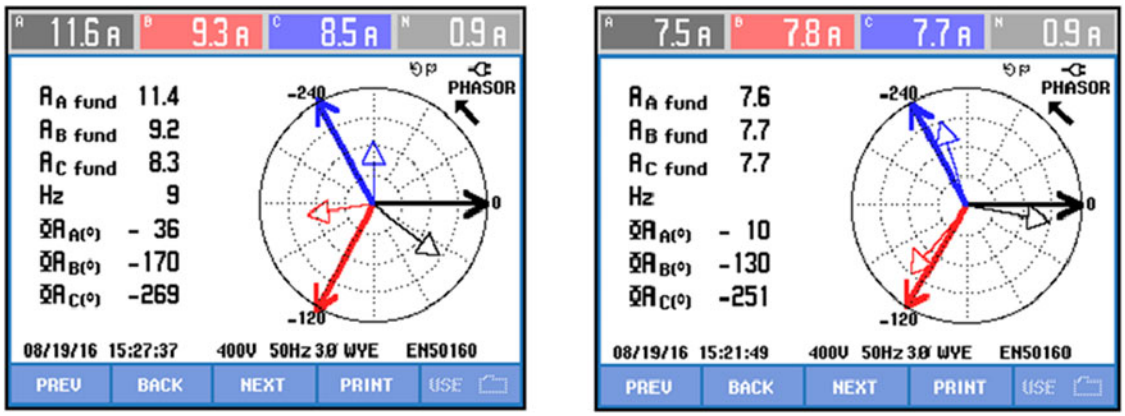

(a) (b)

Fig. 12. Experimental phasor diagrams of v_x and $i_{\rm sx}$: (a) before compensation (b) after the TCLC-HAPF compensation with the proposed selective compensation method ($k_H = 1$, $k_U = 1$, $k_Q = 0.85$).

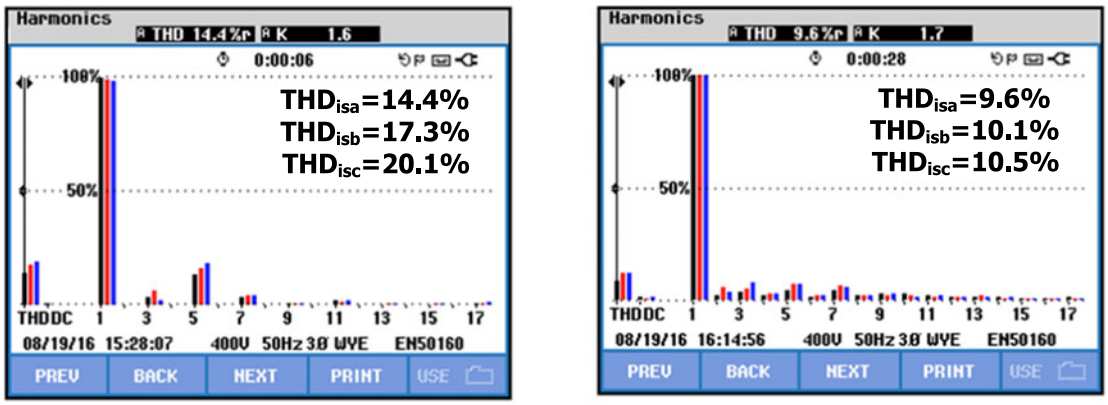

(a) (b)

Fig. 13. Experimental current harmonic spectrums of $i_{\rm sx}$: (a) before compensation (b) after the TCLC-HAPF compensation with the proposed selective compensation method ($k_H = 1$, $k_U = 1$, $k_Q = 0.85$).

VI. Experimental Results

An 110 V-5 kVA experimental prototype of the three-phase three-wire TCLC-HAPF is constructed in the laboratory as shown in Fig. 9. The control system has the sampling frequency of 25 kHz. The switching devices for the active inverter part are Mitsubishi IGBTs PM300DSA060. And, the switching devices for the TCLC part are thyristors SanRex PK110FG160. Moreover, the experimental parameters of the TCLC-HAPF and the test loads are approximately the same as the simulation studies

TABLE IV
EXPERIMENTAL COMPENSATION RESULTS OF THE PROPOSED SELECTIVE COMPENSATION METHOD FOR THE TCLC-HAPF

	Phase	$Q_{\rm sx}$ (var)	PF	$\rm THD_{v\,x}$ (%)	$\rm THD_{isx}$ (%)	$\rm UF_i$ (%)
Before Compensation (see Fig. 10)	*a*	730	0.80	4.5	14.4	32.2
	b	800	0.60	4.5	17.3	
	c	460	0.86	4.6	20.1	
Proposed Selective Compensation ($k_H = 1, k_U = 1, k_Q = 0.85$)	*a*	160	0.98	3.3	9.6	1.3
	b	170	0.98	3.5	10.1	
	c	160	0.98	3.4	10.5	
Before Compensation (see Fig. 14)	*a*	510	0.63	4.5	22.7	29.4
	b	290	0.89	4.5	22.4	
	c	540	0.78	4.6	14.5	
Proposed Selective Compensation ($k_H = 1, k_U = 1, k_Q = 1$)	*a*	50	0.99	3.2	9.4	3.6
	b	50	0.99	3.1	10.5	
	c	40	0.99	3.1	10.5	

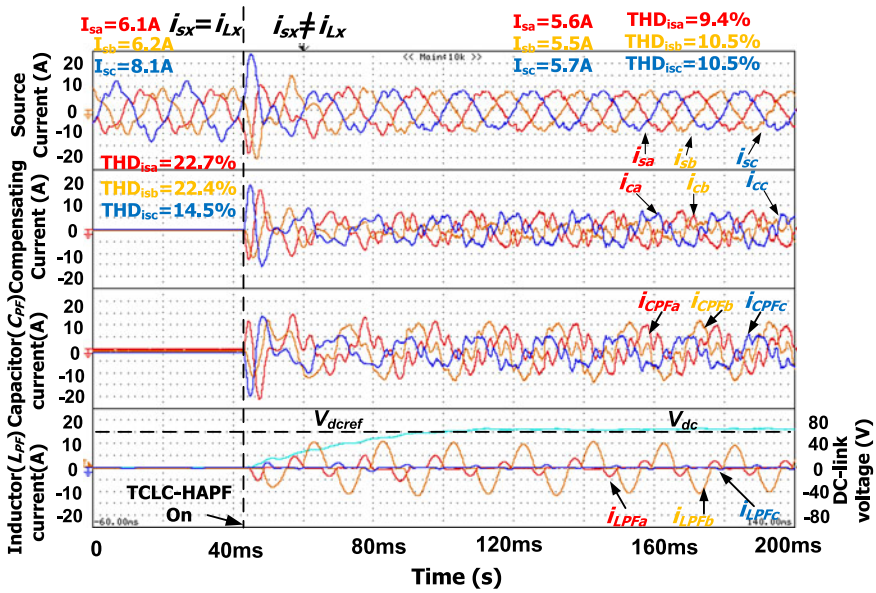

Fig. 14. Experimental waveforms of $i_{\rm sx}$, $i_{\rm cx}$, $i_{\rm CPF}x$, $i_{\rm LPF}x$, and $V_{\rm DC}$ by using the proposed selective compensation method before and after TCLC-HAPF compensation.

in Table II. In addition, during the TCLC-HAPF experimental testing in the laboratory, a small capacity of isolated step-down transformer is used to reduce grid voltage from 230 to 110 V.

Fig. 10 shows the experimental waveforms of the load voltage and source current before and after the TCLC-HAPF compensation with the proposed selective compensation control method ($k_H = 1$, $k_U = 1$, $k_Q = 0.85$). Figs. 11–13 show the experimental results of the source power ($P_{\rm sx}$ and $Q_{\rm sx}$), phasor diagrams, and source current harmonic spectrum, respectively. Table IV also summarizes the corresponding experimental results.

From Fig. 10, it can be seen that after the TCLC-HAPF compensation with the proposed selective compensation method, $i_{\rm sx}$ and v_x are basically in phase with each other. The source PF can be compensated to 0.98 from the original 0.80, 0.86, and 0.86. From Fig. 11, $P_{\rm sx}$ and $Q_{\rm sx}$ in each phase are compensated to about the same (790 W and 160 var) from the original 900, 530, and 780 W for $P_{\rm sx}$ and 730, 800, and 460 var for $Q_{\rm sx}$. And, the remaining $Q_{\rm sx}$ is due to $k_Q = 0.85$ setting. Fig. 12 shows that the magnitude of $i_{\rm sx}$ and phase angle between v_x and $i_{\rm sx}$ of each phase become approximately the same. From Fig. 13, it can be seen that $\rm THD_{isx}$ is improved from 20.1% to 10.5% for the worst phase. From Table IV, $\rm UF_i$ is reduced to 1.3% from the original 32.2%.

Fig. 14 shows the more detailed experimental waveforms of the source currents $i_{\rm sx}$, compensating currents $i_{\rm cx}$, capacitor ($C_{\rm PF}$) currents $i_{\rm CPF}x$, inductor ($L_{\rm PF}$) currents $i_{\rm LPF}x$, and dc-link voltage $V_{\rm dc}$ by using the proposed selective compensation method before and after TCLC-HAPF compensation. Table IV summarizes the corresponding experimental results.

Figs. 15 and 16 provide the dynamic compensation waveforms by applying the proposed selective compensation method for the TCLC-HAPF during voltage dip and voltage fault conditions. From Figs. 15 and 16, they clearly illustrate that the source current can keep sinusoidal and in phase with the load voltage even during the voltage dip and voltage fault conditions.

Comparing the simulation results as in Table III with the experimental results as in Table IV, there are differences between

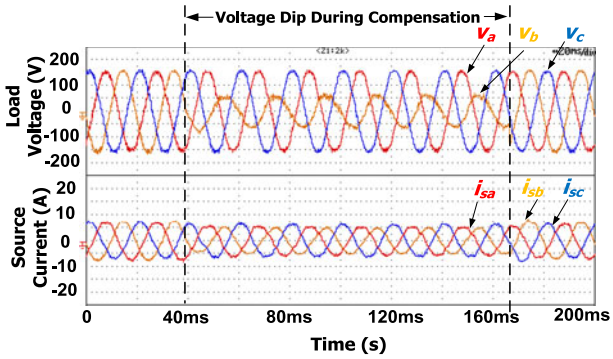

Fig. 15. Dynamic compensation waveforms of v_x and $i_{\rm sx}$ by using the TCLC-HAPF compensation with the proposed selective compensation method during voltage dip.

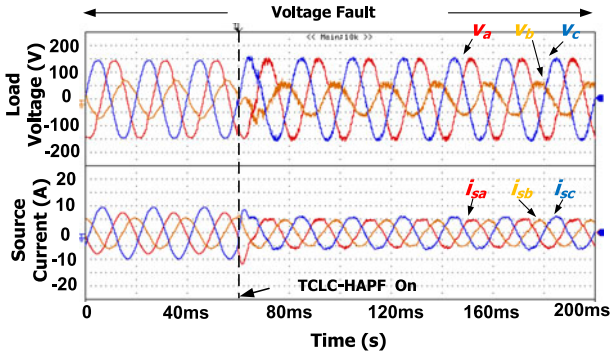

Fig. 16. Dynamic compensation waveforms of v_x and $i_{\rm sx}$ by using the TCLC-HAPF compensation with the proposed selective compensation method during voltage fault.

the simulation and experimental results, which are actually due to the difference of the component parameters, the resolution of the transducers, the digital computation error, and the noise in the experiments. In addition, the small capacity of isolated step-down transformer used in the laboratory also causes larger voltage distortion than the simulation case, which deteriorates the compensation results. Therefore, those factors will affect the TCLC-HAPF compensation performance during experiments.

VII. Conclusion

In this paper, a selective compensation control strategy among distortion, unbalanced and reactive power problems has been proposed for the TCLC-HAPF. The proposed control method can selectively or fully compensate the nonefficient power based on the limited capacity of the TCLC-HAPF. According to the simulation and experimental results, it can be proved that the proposed selective control method can successfully decompose the load power into fundamental positive-sequence reactive/active power, fundamental negative-sequence power (unbalanced power), and harmonic power. And the discomposed power components can be selectively or fully compensated. In addition, the proposed selective compensation method can also function well even at different voltage conditions (e.g., voltage dip).

References

[1] L. Wang, C. S. Lam, and M. C. Wong, "Design of a thyristor controlled LC compensator for dynamic reactive power compensation in smart grid," *IEEE Trans. Smart Grid*, vol. 8, no. 1, pp. 409–417, Jan. 2017.

[2] Y. Liu, W. Wu, Y. He, Z. Lin, F. Blaabjerg, and H. S. H. Chung, "An efficient and robust hybrid damper for LCL- or LLCL-based grid-tied inverter with strong grid-side harmonic voltage effect rejection," *IEEE Trans. Ind. Electron.*, vol. 63, no. 2, pp. 926–936, Feb. 2016.

[3] L. Wang *et al.*, "Non-linear adaptive hysteresis band pulse-width modulation control for hybrid active power filters to reduce switching loss," *IET Power Electron.*, vol. 8, no. 11, pp. 2156–2167, Nov. 2015.

[4] Z. Shuai, A. Luo, J. Shen, and X. Wang, "Double closed-loop control method for injection-type hybrid active power filter," *IEEE Trans. Power Electron.*, vol. 26, no. 9, pp. 2393–2403, Sep. 2011.

[5] L. R. Limongi, L. R. Da Silva Filho, L. G. B. Genu, F. Bradaschia, and M. C. Cavalcanti, "Transformerless hybrid power filter based on a six-switch two-leg inverter for improved harmonic compensation performance," *IEEE Trans. Ind. Electron.*, vol. 62, no. 1, pp. 40–51, Jan. 2015.

[6] R. B. Gonzatti, S. C. Ferreira, C. H. Da Silva, R. R. Pereira, L. E. Borges Da Silva, and G. Lambert-Torres, "Smart impedance: A new way to look at hybrid filters," *IEEE Trans. Smart Grid*, vol. 7, no. 2, pp. 837–846, Mar. 2016.

[7] A. Luo, S. Peng, C. Wu, J. Wu, and Z. Shuai, "Power electronic hybrid system for load balancing compensation and frequency-selective harmonic suppression," *IEEE Trans. Ind. Electron.*, vol. 59, no. 2, pp. 723–732, Feb. 2012.

[8] E. Durna, İ. Yılmaz, and M. Ermiş, "Suppression of time-varying interharmonics produced by medium-frequency induction melting furnaces by a HAPF system," *IEEE Trans. Power Electron.*, vol. 32, no. 2, pp. 1030–1043, Feb. 2017.

[9] J. Dixon, Y. del Valle, M. Orchard, M. Ortuzar, L. Moran, and C. Maffrand, "A full compensating system for general loads, based on a combination of thyristor binary compensator, and a PWM-IGBT active power filter," *IEEE Trans. Ind. Electron.*, vol. 50, no. 5, pp. 982–989, Oct. 2003.

[10] B. Chen, C. Zhang, C. Tian, J. Wang, and J. Yuan, "A hybrid electrical magnetic power quality compensation system with minimum active compensation capacity for V/V cophase railway power supply system," *IEEE Trans. Power Electron.*, vol. 31, no. 6, pp. 4159–4170, Jun. 2016.

[11] A. Luo, Z. Shuai, W. Zhu, and Z. J. Shen, "Combined system for harmonic suppression and reactive power compensation," *IEEE Trans. Ind. Electron.*, vol. 56, no. 2, pp. 418–428, Feb. 2009.

[12] S. Y. Lee and C. J. Wu, "Reactive power compensation and load balancing for unbalanced three-phase four-wire system by a combined system of an SVC and a series active filter," *Proc. Inst. Electr. Eng., Electr. Power Appl.*, vol. 147, no. 6, pp. 563–578, Nov. 2000.

[13] S. Rahmani, A. Hamadi, and K. Al-Haddad, "A combination of shunt hybrid power filter and thyristor-controlled reactor for power quality," *IEEE Trans. Ind. Electron.*, vol. 61, no. 5, pp. 2152–2164, May 2014.

[14] L. Wang, C. S. Lam, and M. C. Wong, "Unbalanced control strategy for a thyristor controlled LC-coupling hybrid active power filter in three-phase three-wire systems," *IEEE Trans. Power Electron.*, vol. 32, no. 2, pp. 1056–1069, Feb. 2017.

[15] L. Wang, C. S. Lam, and M. C. Wong, "A hybrid-STATCOM with wide compensation range and low dc-link voltage," *IEEE Trans. Ind. Electron.*, vol. 63, no. 6, pp. 3333–3343, Jun. 2016.

[16] L. Wang, C. S. Lam, and M. C. Wong, "Hardware and software design of a low dc-link voltage and wide compensation range thyristor controlled LC-coupling hybrid active power filter," in *Proc. TENCON 2015 IEEE Region 10 Conf.*, Nov. 2015, pp. 1–4.

[17] L. Wang, C. S. Lam, and M. C. Wong, "Modeling and parameter design of thyristor controlled LC-coupled hybrid active power filter (TCLC-HAPF) for unbalanced compensation," *IEEE Trans. Ind. Electron.*, 2017, to be published. doi: 10.1109/TIE.2016.2625239.

[18] M. Aleenejad, H. Mahmoudi, P. Moamaei, and R. Ahmadi, "A new fault-tolerant strategy based on a modified selective harmonic technique for three-phase multilevel converters with a single faulty cell," *IEEE Trans. Power. Electron.*, vol. 31, no. 4, pp. 3141–3150, Apr. 2016.

[19] J. He, Y. W. Li, R. Wang, and C. Wang, "A measurement method to solve a problem of using dg interfacing converters for selective load harmonic filtering," *IEEE Trans. Power. Electron.*, vol. 31, no. 3, pp. 1852–1856, Mar. 2016.

[20] Y. Zhang, Y. W. Li, N. R. Zargari, and Z. Cheng, "Improved selective harmonics elimination scheme with online harmonic compensation for high-power pwm converters," *IEEE Trans. Power. Electron.*, vol. 30, no. 7, pp. 3508–3517, Jul. 2015.

[21] X. Zhou, F. Tang, P. C. Loh, X. Jin, and W. Cao, "Four-leg converters with improved common current sharing and selective voltage-quality enhancement for islanded microgrids," *IEEE Trans. Power Del.*, vol. 31, no. 2, pp. 522–531, Apr. 2016.
[22] B. Singh, V. Verma, and J. Solanki, "Neural network-based selective compensation of current quality problems in distribution system," *IEEE Trans. Ind. Electron.*, vol. 54, no. 1, pp. 53–60, Feb. 2007.
[23] B. Singh and V. Verma, "Selective compensation of power-quality problems through active power filter by current decomposition," *IEEE Trans. Power Del.*, vol. 23, no. 2, pp. 792–799, Apr. 2008.
[24] S. Orts-Grau *et al.*, "Selective compensation in four-wire electric systems based on a new equivalent conductance approach," *IEEE Trans. Ind. Electron.*, vol. 56, no. 8, pp. 2862–2874, Aug. 2009.
[25] S. Orts-Grau *et al.*, "Selective shunt active power compensator applied in four-wire electrical systems based on IEEE Std. 1459," *IEEE Trans. Power Del.*, vol. 23, no. 4, pp. 2563–2574, Oct. 2008.
[26] J. C. Alfonso-Gil, E. Pérez, C. Ariño, and H. Beltran, "Optimization algorithm for selective compensation in a shunt active power filter," *IEEE Trans. Ind. Electron.*, vol. 62, no. 6, pp. 3351–3361, Jun. 2015.
[27] IEEE Standard Definitions for the Measurement of Electric Power Quantities Under Sinusoidal, Nonsinusoidal, Balanced, or Unbalanced Conditions, *IEEE Std 1459–2010* (Revision IEEE Std 1459–2000), 2010, pp. 1–52.
[28] D. Yazdani, M. Mojiri, A. Bakhsha,i, and G. JoÓs, "A fast and accurate synchronization technique for extraction of symmetrical components," *IEEE Trans. Power Electron.*, vol. 24, no. 3, pp. 674–684, Mar. 2009.
[29] V. Khadkikar, A. Chandra, and B. N. Singh, "Generalized single-phase p-q theory for active power filtering: simulation and DSP-based experimental investigation," *IET Power Electron.*, vol. 2, pp. 67–78, Jan. 2009.
[30] IEEE Recommended Practices and Requirements for Harmonic Control in Electrical Power Systems, *IEEE Standard 519–2014*, Jun. 2014.
[31] IEEE Recommended Practice for Monitoring Electric Power Quality, *IEEE Std. 1159–2009*, Jun. 2009.
[32] Standardization Administration of the People's Republic of China, GB/T 14549–1993 Power Quality—Harmonics in Public Supply Network. Beijing, China: Electr. Power Press, 1993.
[33] Standardization Administration of the People's Republic of China, GB/T 15543–2008 Power Quality—Three-Phase Voltage Unbalance. Beijing, China: Electr. Power Press, 2008.
[34] Standardization Administration of the People's Republic of China, GB755–87 Rotating Electrical Machines—Rating and Performance. Beijing, China: Electr. Power Press, 1987.
[35] Ministry of Water Resources and Electric Power of China, Regulation of power factor adjustment charge, Beijing, China, 1983.

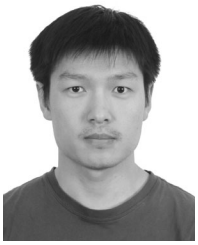

Lei Wang received the B.Sc. degree in electrical and electronics engineering from the University of Macau (UM), Macao, China, in 2011, the M.Sc. degree in electronics engineering from the Hong Kong University of Science and Technology, Hong Kong, China, in 2012, and the Ph.D. degree in electrical and computer engineering from UM, Macao, China, in 2017.

Currently, he is a Postdoctoral Fellow in the Power Electronics Laboratory, UM. His research interests include power electronics, power quality and distribution flexible ac transmission system, power quality compensation, and renewable energy.

Dr. Wang received the champion award in the "Schneider Electric Energy Efficiency Cup," Hong Kong, 2011.

Chi-Seng Lam (S'04–M'12–SM'16) received the B.Sc., M.Sc., and Ph.D. degrees in electrical and electronics engineering from the University of Macau (UM), Macao, China, in 2003, 2006, and 2012 respectively.

From 2006 to 2009, he was an E&M Engineer in UM. In 2009, he simultaneously worked as a Laboratory Technician and started to work toward the Ph.D. degree, and completed the Ph.D. degree within 3 years. In 2013, he was a Postdoctoral Fellow in the Hong Kong Polytechnic University, Hong Kong, China. He is currently an Assistant Professor in the State Key Laboratory of Analog and Mixed-Signal VLSI, UM. He has co-authored 2 books: *Design and Control of Hybrid Active Power Filters* (Springer, 2014) and *Parallel Power Electronics Filters in Three-Phase Four-Wire Systems - Principle, Control and Design* (Springer, 2016), 1 US patent, 2 Chinese patents, and more than 50 technical journals and conference papers. His research interests include integrated power electronics controllers, power management integrated circuits, power quality compensators, smart grid technology, renewable energy, etc.

Dr. Lam received the Macao Science and Technology Invention Award (Third-Class) and the R&D Award for Postgraduates (Ph.D.) in 2014 and 2012, respectively, the Macao Government Ph.D. Research Scholarship in 2009–2012, the Macao Foundation Postgraduate Research Scholarship in 2003–2005, and the 3rd RIUPEEEC Merit Paper Award in 2005. In 2007, 2008, and 2015, he was the GOLD Officer, a Student Branch Officer, and the Secretary of IEEE Macau Section. He is currently the Vice-Chair of IEEE Macau Section and the Secretary of IEEE Macau PES/PELS Joint Chapter. He was the Local Arrangement Chair of IEEE TENCON 2015 and ASP-DAC 2016.

Man-Chung Wong (SM'06) received the B.Sc. and M.Sc. degrees in electrical and electronics engineering from the University of Macau (UM), Macao, China, in 1993 and 1997, respectively, and the Ph.D. degree in electrical engineering from Tsinghua University, Beijing, China, in 2003.

He was a Visiting Fellow in Cambridge University, Cambridge, U.K., in 2014. He is currently an Associate Professor in the Department of Electrical and Computer Engineering, UM. He has co-authored 2 Springer books, more than 100 journal and conference papers, and 6 patents (China and USA). Recently, an industrial power filter platform was developed and installed in a practical power system based on his research results. His research interests include power electronics converters, pulse with modulation, active power filters, hybrid active power filters, and hybrid power quality compensator for high-speed railway power supply system.

Dr. Wong received the Macao Young Scientific Award from the Macau International Research Institute in 2000, the Young Scholar Award of UM in 2001, Second Prize for the Tsinghua University Excellent Ph.D. Thesis Award in 2003, and the Macao Science and Technology Invention Award (Third-Class) in 2012 and 2014. He supervised several students to receive merit paper awards in conferences and champions in student project competitions. He was several conference committee members and the General Chair of IEEE TENCON 2015 in Macau. In 2014–2015, he was the IEEE Macau Section Chair. Currently, he is the North Representative of IEEE Region 10 Power and Energy Society and the IEEE Macau PES/PELS Joint Chapter Chair.